Physica Scripta. Vol. T23, 227–231, 1988.

# Unipolar Hot Electron Transistors

A. F. J. Levi[1] and T. H. Chiu[2]

[1]AT&T Bell Laboratories, Murray Hill, New Jersey, U.S.A.; [2]AT&T Bell Laboratories, Holmdel, New Jersey, U.S.A.

*Received August 10, 1987; accepted November 26, 1987*

**Abstract**

We discuss kinematic and dynamical constrains in design of useful unipolar hot electron transistors. In addition, we demonstrate room temperature operation of a double heterojunction hot electron transistor with a two-dimensional electron gas forming the base region. Our test structure has the narrowest ever reported base width at a mere 100 Å and is the first such transistor to show current gain in excess of 10 at room temperature. The device uses an indirect, wide bandgap $AlSb_{0.92}As_{0.08}$ emitter and the transistor base is a thin InAs layer.

## 1. Introduction

Since the invention of the bipolar transistor (Ref. [1]) various attempts have been made to develop new types of transistor in which charge transport is non-diffusive. For example, in the 1960's metal-base and "ballistic" electron transistors were proposed for high speed applications. Unfortunately, materials problems and strong electron scattering severely limited the performance of these devices to common emitter current gain of less than unity [2]. These early failures reduced interest in developing novel transistors and work in this area declined.

In 1979, advances in semiconductor processing technology enabled Shannon to realize a unipolar Hot Electron Transistor (HET) in silicon using ion implantation to define abrupt p–n junctions [3]. In 1980, Malik *et al.* used the precise doping profiles obtainable by molecular beam epitaxy (MBE) to form two back to back "planar doped barriers" and fabricated the first unipolar HET in GaAs [4]. Although these early devices did not exhibit significant current gain (even when operated at liquid helium temperature) there was renewed interest in developing HETs and, in particular, to understand the physics of nonequilibrium electron transport in semiconductors over length scales of order 100 Å [5]. However, there always remained the lingering hope that a useful, unipolar HET operating at room temperature would be possible.

## 2. Unipolar hot electron transistors

### 2.1. *Design Considerations*

There are similarities between a unipolar HET and an n–p–n double heterojunction bipolar transistor. Both, for example, have high current drive capability. However, in contrast to the bipolar, for a given geometry, the unipolar HET has a very low base resistance, $R_b$ due to approximately two orders of magnitude greater electron mobility, compared to hole mobility in typical III–V semiconductors. In principle, a unipolar transistor also has low forward bias emitter-base capacitance, $C_{eb}$ due to the absence of minority carrier diffusion effects. Hence, the $R_bC_{eb}$ time constant limiting bipolar speed is unimportant in a suitably designed unipolar HET allowing the possibility that ultimate device speed depend only upon the hot electron emitter- collector transit time. For this reason there is some interest in developing unipolar HETs for high speed electronics applications [6–8].

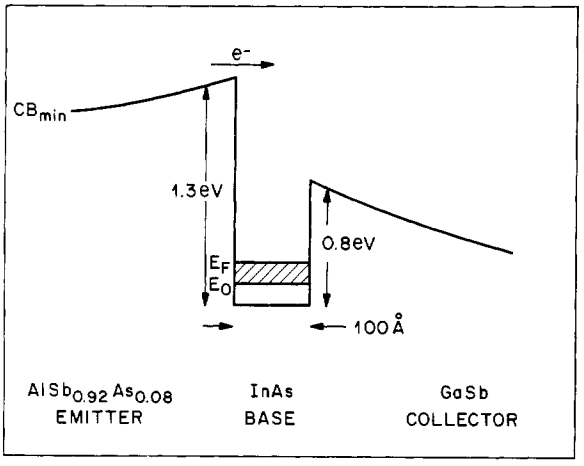


*Fig. 1.* Schematic diagram of the conduction band of an $AlSb_{0.92}As_{0.08}$/InAs/GaSb double heterojunction unipolar HET under bias. The conduction band minimum, $CB_{min}$ is indicated as is the confinement energy, $E_0$ and the Fermi energy, $E_F$ of the occupied two dimensional electron states in the InAs base.

In Fig. 1 we show a schematic diagram of the conduction band of a (001) oriented, $AlSb_{0.92}As_{0.08}$/InAs/GaSb double heterojunction unipolar HET under bias. The use of a wide band gap $AlSb_{0.92}As_{0.08}$ emitter allows room temperature operation because, unlike previous HETs, electrons are injected approximately 1.3 eV above the conduction band minimum of the base which is more than 50 times greater than ambient thermal energies of around 0.025 eV. The transistor base consists of a 100 Å thick epilayer of InAs with a carrier concentration of two dimensionally confined electrons, $n \sim 2 \times 10^{12}\,cm^{-2}$. The collector arm is 3500 Å of Te doped ($n \sim 1 \times 10^{16}\,cm^{-3}$) GaSb and the entire epilayer structure is grown by molecular beam epitaxy on a (001) oriented n-type GaSb substrate.

To utilize the HET's high current drive capability (useful for high speed applications) we use thermionic emission to inject electrons of energy $E_i$ from the emitter into the base. Space charging effects can occur in the emitter and collector barriers when the device is operated at high current density. This is avoided by doping the barriers to a density $n > j/ev$ where $v$ is the average velocity in the barrier, $j$ is the current density and $e$ the electron charge. Reverse current flow from base to emitter and collector to base is minimized by choosing emitter barrier energy $\phi_{eb}$ ($\cong E_i$) and collector barrier $\phi_{bc}$ to be much greater than ambient thermal energy $k_BT \cong 0.025$ ev (typically we require $\phi_{bc} \gtrsim 0.5$ eV).

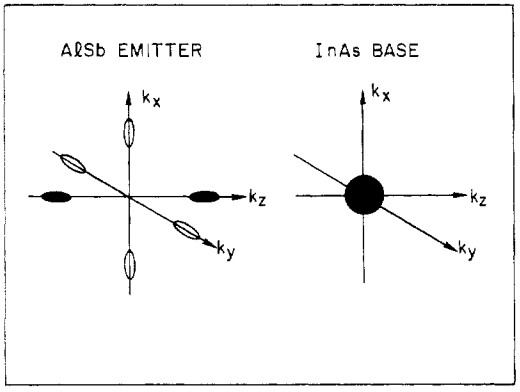


*Fig. 2.* Kinematic constraints result in only electrons in the shaded X-minimum $AlSb_{0.92}As_{0.08}$ conduction band pockets being injected into the shaded unoccupied Γ-states in the InAs base.

Consider a thermal electron injected from a state close to the X-minimum of the $AlSb_{0.92}As_{0.8}$ conduction band in the emitter into a Γ-state of energy $E_i$ in the InAs base. Because, in the absence of scattering, the injection process conserves energy, $E_i$, and wave vector parallel to the interface, $k_\parallel$, band structure considerations dictate that electrons cannot be injected into large $k_\parallel$ states. The kinematic constraints giving rise to this type of injection window are illustrated in Fig. 2. Only electrons in the shaded X-minimum $AlSb_{0.92}As_{0.08}$ conduction band pockets are injected into the unoccupied Γ-states in the InAs base. An approximate measure of the spread in injection angles is given by $\Delta\theta = \tan^{-1}(k_B T/E_i)^{1/2}$. For our device this gives $\Delta\theta \sim 8°$ at room temperature. The injected electrons therefore traverse the base in the minimum possible time with a large component of momentum in the $z$ direction, perpendicular to the interface.

It is important to inject electrons in a narrow range of energies close to $E_i$. Optimum device performance occurs when quantum reflections from $\phi_{bc}$ are minimized and this can only be achieved for a limited range of injection energies. This point may be illustrated using the established boundary conditions employed in the effective mass approximation [9]. Reflections from the abrupt change in potential at $\phi_{bc}$ approach zero when the hot electron velocity (more generally the slope $\partial\omega/\partial k$ at energy $E_i$ in Fig. 3) is the same either side of the base-collector junction [8]. This impedance matching condition is $m_1^*/m_2^* = E_i/(E_i - \phi_{bc})$, where $m_1^*$ and $m_2^*$ are the effective electron masses in the base and collector respectively. Therefore, by carefully choosing $E_i$, $\phi_{bc}$, base and collector materials, including the possible use of superlattices, quantum reflections from $\phi_{bc}$ can be eliminated for a small range ($\sim 0.5$ eV) of $E_i$. It is worth mentioning that at a real heterojunction interface, impedance matching also requires that the character of the electron wave function in the base and collector be similar (for example the Γ, *s*-like states at energy $E_i$ in Fig. 3).

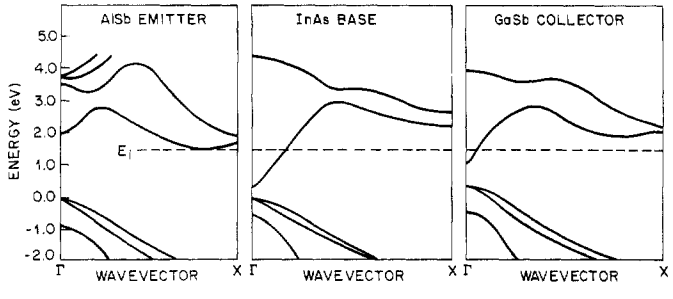


*Fig. 3.* Band diagrams illustrating the states used in (001) transmission of an electron energy $E_i$ through an AlSb/InAs/GaSb double heterostructure unipolar HET.

Although quantum mechanical reflection is not a fundamental limit to device performance it is known that inelastic electron scattering is. This dynamical constraint applies to both unipolar [6] and bipolar [10] HETs. Calculations indicate that, for a given resistivity of ambient carriers, scattering rates in bulk InAs are almost a factor of two less than in GaAs. This is due to a reduced density of states in InAs compared to GaAs (InAs has an effective electron mass $m^*_{InAs} = 0.021\,m_0$ whereas GaAs has $m^*_{GaAs} = 0.07\,m_0$). In addition to choosing a low effective electron mass material for the base, scattering can be reduced by decreasing the base width.

A transistor base in which ambient electrons occupy two-dimensional electronic states has a number of advantages. For example, it is known that enhanced electron mobility may be achieved in such a system [11] thereby reducing the base resistance, $R_b$. Of greater significance, however, are the constrains on scattering imposed by the quantization of electronic states in the base.

An injected electron, energy $E_i$ and wave vector $\boldsymbol{k}_i$, moving in the $z$ direction is able to scatter into a continuum of high energy states in the base by losing energy $\hbar\omega$ and changing wave vector by $\boldsymbol{q}$. For example, small angle Coulombic scattering due to emission of longitudinal polar optical phonons is possible and occurs with a probability close to that in the bulk. However, energy and momentum conservation restrict electron-electron scattering in the base. As illustrated in Figs. 4 and 5, quantization limits the type of electronic excitations which can occur and, because Coulomb scattering is predominantly small angle, the probability of electron-electron scattering from occupied two-dimensional electronic states in the base is less than the corresponding bulk value.

There are other, potentially important scattering mechanisms which can limit performance of a HET. For example, above a critical value of injection energy, $E_i$ there is a high probability of electron transfer into the subsidiary X-minima

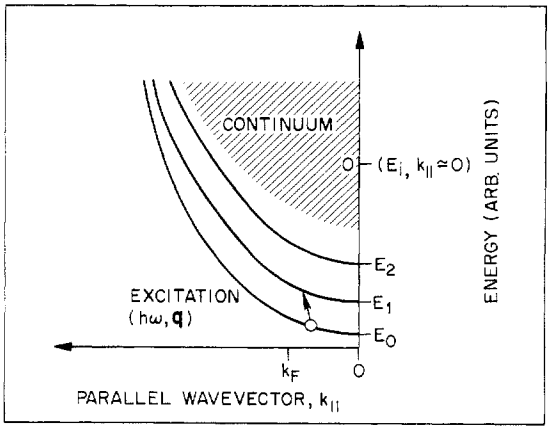


*Fig. 4.* Schematic diagram showing excitation of a conduction band electron between subbands in the base. The subbands have quantization energies $E_0$, $E_1$, and $E_2$. The excitation is characterized by an energy $\hbar\omega$ and wave vector $\boldsymbol{q}$.

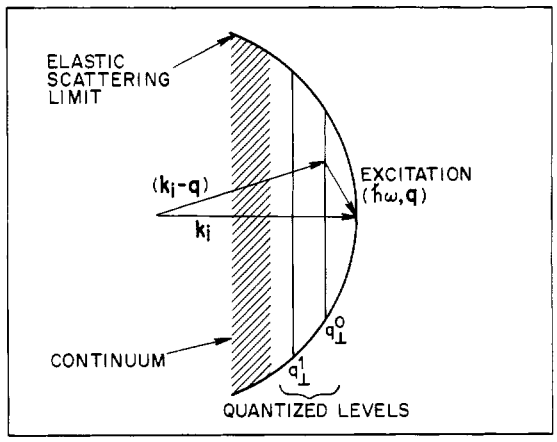


*Fig. 5.* Illustration of restrictions imposed on scattering by quantization of electronic states in the transistor's base. The injected electron has initial energy $E_i$, wave vector $k_i$ and is scattered, changing wave vector by $q$ and losing energy $\hbar\omega$. The elastic scattering limit, in which the injected electron changes wave vector but maintains its energy, is indicated. For the sake of simplicity, we do not consider the small ($\sim 30\%$) contribution to scattering at room temperature in which the injected electron gains energy.

in InAs. However, as may be seen in Fig. 3, in our structure $E_i$ is more than 0.5 eV *below* the energy of the subsidiary X-minimum so this scattering mechanism is unimportant in our device. Another scattering mechanism which should be considered arises due to the small band gap, $E_g$ of low effective electron mass materials such as InAs. A conduction band electron of energy $E_i \gg E_g$ can excite an electron from the valence band into the conduction band [12]. However, the confinement energy, $E_0$ and the Fermi energy, $E_F$ of electrons in the 100 Å wide base serves to increase the band gap of InAs from 0.36 eV to an effective value of around 0.6 eV while retaining the advantage of the semiconductor's low effective electron mass. This increase in effective band gap greatly reduces the probability of direct excitation from the valence band.

### 2.2. *Crystal growth*

The epitaxial layer structure shown in Fig. 1 is grown in an MBE system on (001)-oriented Te-doped GaSb substrates using elemental sources [13]. The growth temperature is 560°C for InAs, as determined by an optical pyrometer. For HETs with a 100 Å wide InAs base, it is essential to have atomically smooth heterointerfaces with minimal interfacial defects. One major problem in growing abrupt (Al, Ga)Sb/InAs heterointerfaces involves changing the group V species during growth. To stabilize the growth at the temperatures of interest, it is necessary to use high group V overpressures which leads to high background pressures of As and Sb. This sitution is difficult to avoid if mechanical shutters are used to control the group V flux. The coexistence of both species in the growth front of InAs or (Al, Ga)Sb may cause the exchange of As and Sb at the surface leading to localized compositional fluctuations or even 3-dimensional growth at the interface. use of antimony and arsenic dimers, obtained by means of cracking the respective tetramers in the high temperature zone of the ovens, improves the incorporation efficiency of group V elements and helps cut down the group V overpressure required for growth.

Reflection high energy electron diffraction (RHEED) is used to monitor the transition at each heterointerface. Abrupt interfaces are characterized by the immediate transition of the reconstruction pattern from (1 × 1) for InAs to (1 × 3) for (Al, Ga)/Sb, and vice versa, without any 3-dimensional nucleation stage. The thickness of the strained InAs layer is kept below 200 Å, ensuring commensurate growth. The lattice mismatch of $6 \times 10^{-3}$ between InAs and GaSb is accommodated by elastic deformation of the InAs lattice in the narrow base region. This elastic deformation modifies the valence band structure in a known way [14] but has little effect on the conduction band and so its effect on electrical measurements can be ignored. For the 1500 Å thick AlSb emitter region, there is a tendency to develop some dislocations which can be removed with the addition of As to form $AlSb_{0.92}As_{0.08}$, thereby improving the lattice match to the GaSb substrate. The as-grown wafers show excellent specular morphology under Nomarksy microscopy.

We have also grown similar, high quality, InAlGaAsSb structures on GaAs substrates and we note that there appears to be no fundamental obstacle to epitaxial growth on Si substrates [15].

### 2.3. *Preliminary results and discussion*

After removal from the growth chamber wafers are fabricated into a two level mesa structure allowing emitter, base and collector to be contacted individually and the device characteristics measured. Special mention should be made concerning contact to the transistor base. This is achieved using the natural electron accumulation layer occuring at the exposed InAs surface. We use a 400 Å thick AuGe alloy for contact metalization and the alloy is annealed for a few seconds at 230°C in a hydrogen atmosphere. Following this, Ti/Au metalization is deposited and samples are wire bonded onto standard 16-pin packages for convenient electrical characterization.

In Fig. 6(a) and (b) typical measured common base current gain, $\alpha$ and common emitter current gain, $\beta$ are shown for a device maintained at a temperatre $T = 300$ K [8]. Although there is good agreement between the $\alpha$ and $\beta$ measurements, the saturation characteristics are non-ideal exhibiting a small slope with increasing collector voltage bias. As may be seen in Fig. 6(b), the room temperature value of $\beta$ increases from $\beta = 10$ at $V_{ce} = 1.0$ V to $\beta = 17$ at $V_{ce} = 3.0$ V. At liquid nitrogen temperature $\beta = 12$ at $V_{ce} = 1.0$ V and $\beta = 40$ at $V_{ce} = 3.0$ V. We note that the reduction in base/collector potential barrier, $\phi_{bc}$ with increasing collector voltage bias,

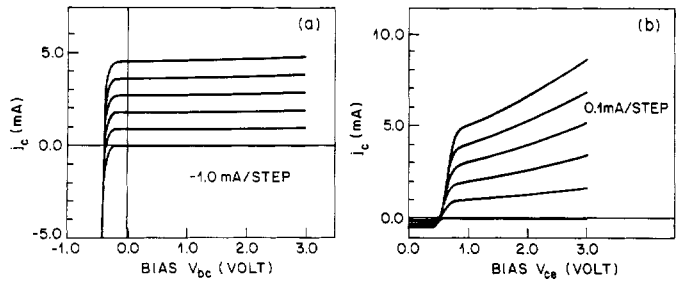


*Fig. 6.* (a) Room temperature ($T = 300$ K) common base current gain characteristics of the device shown schematically in Fig. 1. Curves were taken in steps of $-1.0$ mA beginning with an injected emitter current of zero. (b) Room temperature common emitter current gain characteristics of the device in Fig. 2(a). Curves were taken in steps of 0.1 mA beginning with an injected base current of zero. Emitter area is $7.8 \times 10^{-5}$ cm$^{-2}$, $j_c$ is collector current, and $V_{ce}$ is collector-emitter voltage bias.

$V_{cc}$ improves collector efficiency for incoming hot electrons and, in agreement with simple calculations, contributes to the observed slope in the common emitter saturation characteristics. In addition, careful analysis of emitter, base and collector current in different biasing configurations reveals that ionization by hot carriers in the collector is unimportant for low values of $V_{ce}$ but dominates the gain characteristics for $V_{ce} \gtrsim 4.0\,V$. We therefore obtain a lower limit for current gain in the transistor by measuring $\beta$ at a bias of $V_{ce} \sim 1.0\,V$ which is just above the threshold offset voltage, $V_{ce}(\text{offset}) \sim 0.5\,V$. Using this criterion and to confirm the high current drive capability of the device we have measured $\beta = 10$ for collected current of less than 1 mA to 100 mA (corresponding to current densities from less thn $10\,A\,cm^{-2}$ to more than $1200\,A\,cm^{-2}$).

The electrical characteristics of the device may be described using a phenomenological model [16]. In this model the transistor is considered as two back to back Schottky diodes in which a fraction, $\alpha$ of the emitter current, $j_e$ flows in the collector as collector current, $j_c$. Assuming the ideality, $n$ of the emitter-base and base-collector junctions are the same then the offset voltage in the common-emitter current gain characteristics is given by

$$V_{ce}(\text{offset}) \sim \frac{nk_B T}{e} \ln (j_{c0}/\alpha j_{e0})$$

where $j_{c0}$ and $j_{e0}$ are the collector and emitter revese bias saturation currents respectively. At a temperature $T = 300\,K$ this gives $V_{ce}(\text{offset}) \sim 0.5\,V$ for $\phi_{bc} = -0.6\,eV$ and $\phi_{eb} = -1.1\,eV$ which is in agreement with the experimental observations (see Fig. 6(b)).

In Fig. 7 we show the calculated common emitter current gain, $\beta$ characteristics, of our device. In this simulation $\alpha = 0.91$ giving a current gin $\beta \sim 10$. There is reasonable overall agreement between the experimental results shown in Fig. 6(b) and the calculated characteristics shown in Fig. 7. However, the model is unable to reproduce the increase in $\beta$ with increasing bias, $V_{ce}$ because in our simple model $\alpha$ is a constant, independent of $V_{ce}$.

As mentioned in Section 2.1, quantum reflections from $\phi_{bc}$ can limit device performance. The importance of these reflections from $\phi_{bc}$ can limit device performance. The importance of these reflections can be explored experimentally by replacing the $AlSb_{0.92}As_{0.08}$ emitter with GaSb as illustrated in Fig. 8(a). The measured common emitter current gain of such a symmetric device is shown in Fig. 8(b). As may be seen, near threshold $\beta$ is around 1.3 corresponding to more than 43% of injected electrons being trapped in the base region and contributing to base current. This dramatic decrease in $\beta$ illustrates the detremental effect quantum reflections have on device performance and highlights the need to eliminate reflections by impedance matching current carrying states across the abrupt base-collector heterojunction.

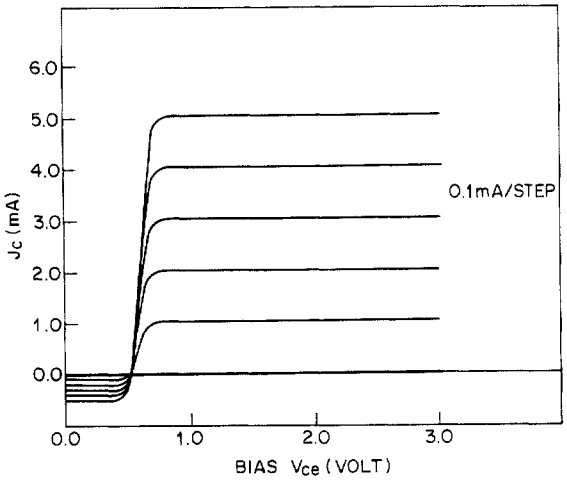


*Fig. 7.* Calculated room temperature ($T = 300\,K$) common emitter current gin characteristics. The base transport factor is $\alpha = 0.91$.

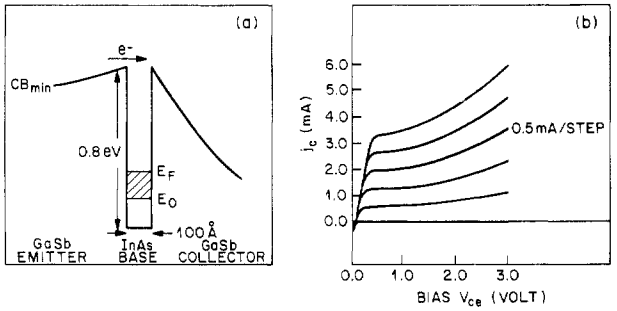


*Fig. 8.* (a) Schematic diagram of the conduction band of a symmetric GaSb/InAs/GaSb double heterojunction unipolar HET under bias. (b) Room temperature common emitter current gain of the device shown schematically in Fig. 8(a). Curves were taken in steps of 0.5 mA beginning with an injected base current of zero.

## 3. Concluding remarks

We have demonstrated room temperature operation of a double heterojunction unipolar transistor with high current drive capability and common emitter current gain, $\beta$ greater than 10. This was achieved using a wide bandgap, $AlSb_{0.92}As_{0.8}$ emitter and a 100 Å wide InAs base.

These preliminary results are encouraging. However, room temperature values of $\beta$ have to be increased before unipolar HETs can be considered a realistic option in ultrafast circuit design. The immediate technological significance of our work is in establishing the electrical quality of the InAlGaAsSb material system as this material system has important advantages for HETs, field effect and bipolar transistors as well as various opto-electronic applications.

In addition to technological issues, there are also questions about the basic physics underlying HET operation. Unfortunately, little is known about the physics of nonequilibrium electron transport on a 100 Å length scale in semiconductors. For example, it is known that hot electron scattering rates in the base present a fundamental limit to HET device performance [6, 10]. However, a satisfactory theory which describes scattering rates for perpendicular transport across a two dimensional electron gas has yet to be formulated. We note that any such theory must address two competing effects; first, the reduction, compared to the three dimensional case, in screening which will tend to increase scattering rates and second, the small scattering angles, typical of Coulomb scattering, which will tend to decrease scattering rates for perpendicular transport.

Another issue concerns the correct description of electron scattering in the presence of large electric fields. A quantum mechanical treatment of the Boltzmann transport equation leads to the intra-collisional field effect for electric fields greater than around $10^4\,V\,cm^{-1}$ [17]. This invalidates the use of the Golden Rule to calculate scattering rates in high elec-

tric fields. It therefore becomes important to know if an electron traversing an abrupt heterojunction experiences a dramatic change in scattering rate because, although the interaction volume is very small, the electric field is non-uniform and very large.

From the above discussion is should be obvious to the reader that much remains to be done!

## Acknowledgements

We wish to thank D. R. Hamann and S. Schmitt-Rink for useful discussions.

## References

1. Bardeen, J. and Brattain, W. H., Phys. Rev. **75**, 1208 (1949); Shockley, W., Bell System Tech. J. **28**, 435 (1949).
2. For a review of this early work see Sze, S. M., "Physics of Semiconductor Devices," New York: Wiley, 1981.
3. Shannon, J. M., IEE J. Solid State Electron Devices **3**, 142 (1979); Shannon, J. M. and Gill, A., Electron. Lett. **17**, 620 (1981).
4. Malik, R. J., AuCoin, T. R., Ross, R. L., Board, K., Wood, C. E. C. and Eastman, L. F., Electron. Lett. **16**, 836 (1980); Malik, R. J., Hollis, M. A., Eastman, L. F., Woodward, D. J., Wood, C. E. C. and AuCoin, T. R., Proc. Conf. Active Microwave Devices, Cornell Univer., Ithaca, NY, 1981, p. 87.
5. For a review of this early work see Hayes, J. R. and Levi, A. F. J., IEEE J. Quantum Electron, **22**, 1744 (1986).
6. Levi, A. F. J., Hayes, J. R. and Bhat, R., Appl. Phys. Lett. **48**, 1609 (1986).
7. Imamura, K., Muto, S., Fujii, T., Yokoyama, N., Hizamizu, S. and Shibatomi, A., Electron Lett. **22**, 1148 (1986).
8. Levi, A. F. J. and Chiu, T. H., Appl. Phys. Lett. **51**, 984 (1987).
9. See, for example, Ando, Y. and Itoh, T., J. Appl. Phys. **61**, 1497 (1987).
10. Levi, A. F. J. and Yaffet, Y., Appl. Phys. Lett. **51**, 42 (1987).
11. Dingle, R., Störmer, H. L., Gossard, A. C. and Wiegmann, W., Appl. Phys. Lett. **33**, 665 (1978).
12. Glicksman, M. and Steele, M. C., Phys. Rev. **110**, 1204 (1958).
13. Tsang, W. T., Chiu, T. H., Kisker, D. W. and Ditzenberger, J. A., Appl. Phys. Lett. **46**, 283 (1985); Chiu, T. H., Tsang, W. T. and Levi, A. F. J., Electron. Lett. **23**, 917 (1987).
14. Pollak, F. H., Surface Science **37**, 863 (1973); Chang, Y. C., Chu, H. Y., and Chung, S. G., Phys. Rev. **B33**, 7364 (1986); O'Reilly, E. P. and Witchlow, G. P., Phys. Rev. **B34**, 6030 (1986).
15. Malik, R. J., van der Ziel, J. P., Levine, B. F., Betha, C. G. and Walker, J., Appl. Phys. Lett. **59**, 3909 (1986).
16. Chand, N., Fischer, R. and Morkoc, H., Appl. Phys. Lett. **47**, 313 (1985).
17. Barker, J. R., and Ferry, D. K., Phys. Rev. Lett. **42**, 1179 (1979); Khan, F. S., Davies, J. H. and Wilkins, J. W., Phys. Rev. **B36**, 2578 (1987).